

Different Single-Photon Response of Wide and Narrow Superconducting $\text{Mo}_x\text{Si}_{1-x}$ Strips

Yu. P. Korneeva^{1,*}, N.N. Manova¹, I.N. Florya,¹ M. Yu. Mikhailov², O.V. Dobrovolskiy^{3,4},
A.A. Korneev^{1,5} and D. Yu. Vodolazov^{1,6}

¹*Physics Department, Moscow Pedagogical State University, Moscow 119991, Russia*


²*B. Verkin Institute for Low Temperature Physics and Engineering of the National Academy of Sciences of Ukraine, Kharkiv 61103, Ukraine*

³*Faculty of Physics, University of Vienna, 1090 Vienna, Austria*

⁴*Physics Department, V. Karazin Kharkiv National University, Kharkiv 61022, Ukraine*

⁵*National Research University Higher School of Economics, Moscow 101000, Russia*

⁶*Institute for Physics of Microstructures, Russian Academy of Sciences, Nizhny Novgorod GSP-105, Russia*

 (Received 3 October 2019; revised manuscript received 28 November 2019; accepted 29 December 2019; published 6 February 2020)

The photon count rate (PCR) of superconducting single-photon detectors made of $\text{Mo}_x\text{Si}_{1-x}$ films shaped as a $2\text{-}\mu\text{m}$ -wide strip and a 115-nm -wide meander strip line is studied experimentally as a function of the dc biasing current at different values of the perpendicular magnetic field. For the wide strip, a crossover current I_{cross} is observed, below which the PCR increases with an increasing magnetic field and above which it decreases. This behavior contrasts with the narrow $\text{Mo}_x\text{Si}_{1-x}$ meander, for which no crossover current is observed, thus suggesting different photon-detection mechanisms in the wide and narrow strips. Namely, we argue that in the wide strip the absorbed photon destroys superconductivity *locally* via the vortex-antivortex mechanism for the emergence of resistance, while in the narrow meander superconductivity is destroyed across the whole strip line, forming a hot belt. Accordingly, the different photon-detection mechanisms associated with vortices and the hot belt determine the qualitative difference in the dependence of the PCR on the magnetic field.

DOI: [10.1103/PhysRevApplied.13.024011](https://doi.org/10.1103/PhysRevApplied.13.024011)

I. INTRODUCTION

Recently, it has been reported that single-photon response in NbN thin films occurring in the well-known narrow and long meandering nanowires [1,2] also occurs in constrictions that are a few microns wide and/or tapered [3]. This experimental finding is an indirect indication of the applicability of the vortex-antivortex-assisted mechanism for single-photon counting, which was introduced in the theoretical work by Zotova and Vodolazov (ZV) [4,5]. In the ZV model, the only requirement is that the superconducting bridge carries over its width a uniform bias current, the value of which is close to the critical pair-breaking one. Thus, this requirement ensures that the bridge operates in a “local” regime. Namely, whenever a photon hits the bridge, creating a local nonequilibrium state (which is often called a “hot spot”), the supercurrent density distribution is changed inside and close to the “impact point” and it is not perturbed further away. Then, a vortex-antivortex pair is created and driven by the Lorentz

force, causing the emergence of dissipation in the superconductor. In this mechanism, each point of the bridge contributes to photon counting and the intrinsic detection efficiency is predicted to reach almost 100%. Specifically, the ZV model requires the bias current in the bridge to roughly exceed half of the depairing current. Previously, these conditions have been experimentally satisfied in wide and short NbN bridges studied by Korneeva *et al.* [3]. The experimental observations have been consistent with the ZV model for the vortex-assisted mechanism of initial dissipation [4]. While that work has offered micrometer-wide NbN bridges as an alternative to the standard superconducting single-photon detectors, based on nanometer-scale nanowires implemented in long meandering structures, the applicability of the ZV model to superconductors with weaker pinning has lacked experimental scrutiny so far.

Here, we study experimentally the magnetic field dependent photon count rate (PCR) of a $2\text{-}\mu\text{m}$ -wide and $10\text{-}\mu\text{m}$ -long superconducting strip in comparison with a 115-nm -wide meander strip line made of $\text{Mo}_x\text{Si}_{1-x}$, an important superconducting-thin-film material that is widely used in highly efficient superconducting single-photon detectors [6,7]. In addition to weak pinning,

*korneeva@rplab.ru

$\text{Mo}_x\text{Si}_{1-x}$ is chosen for the sake of achieving larger experimental critical currents, the values of which should be close to the critical pair-breaking current in the material, for the high detection efficiency. By carrying out experiments at different values of the perpendicular magnetic field, we provide a more direct test of the vortex-antivortex model, since the applied magnetic field breaks the translation symmetry for the creation of a vortex-antivortex pair and the current distribution, because the latter is no longer uniform over the cross section of the bridge. In addition to the wide $\text{Mo}_x\text{Si}_{1-x}$ strip, we also study the single-photon response of a narrow meandering $\text{Mo}_x\text{Si}_{1-x}$ strip line, where an absorbed photon is capable of suppressing superconductivity across its whole width (creating the so-called “hot belt”) and the “local” response is not expected.

Our key observation for the wide $\text{Mo}_x\text{Si}_{1-x}$ strip is that the PCR has a crossover current below which it increases with the magnetic field and above which it decreases. Since a similar crossover in the presence of a magnetic field has been observed previously in submicrometer-wide NbN strips, we believe that the same vortex-assisted mechanism is at work in those narrow strips [8]. By contrast, we do not observe a crossover current for the $\text{Mo}_x\text{Si}_{1-x}$ meander strip line, although we reveal a saturation of the PCR at large values of the bias current. This finding implies that in the narrow $\text{Mo}_x\text{Si}_{1-x}$ strip (the width of which is comparable with the width of the NbN strip in Ref. [8]), the absorbed photon suppresses superconductivity across the whole width of the superconductor, which leads to a different dependence of the PCR on the magnetic field.

II. EXPERIMENT

The $\text{Mo}_{68}\text{Si}_{32}$ films are deposited by dc magnetron cosputtering of elemental molybdenum and silicon targets onto Si wafers covered with a 230-nm-thick SiO_2 layer [9]. The atomic percent composition of the $\text{Mo}_{68}\text{Si}_{32}$ films is ensured by using the calibrated deposition rates in conjunction with x-ray reflectivity measurements for deduction of the film thickness. Here, we report the results for a straight strip and a meander strip line made of 3.3-nm-thick films that have a superconducting transition temperature T_c of 3.85 K. From the extrapolation of the linear section of the upper critical magnetic field B_{c2} near T_c , we estimate an electron-diffusion coefficient of $D = 0.47 \text{ cm}^2 \text{ s}^{-1}$ [10] and $B_{c2}(0)$ as 8.66 T, yielding the zero-temperature coherence length $\xi_c(0) \approx 8.7 \text{ nm}$. The one-spin electronic density of states $N_0 = 2.51 \times 10^{24} \text{ m}^3 \text{ K}^{-1}$ is deduced from the Einstein relation. The theoretical depairing current I_{dep} at a given temperature is determined from the approximate expression for the critical depairing current, $I_{\text{dep}}(T) = I_{\text{dep}}(0)[1 - (T/T_c)^2]^{3/2}$, the applicability of which for dirty superconductors is justified by Clem and Kogan [11], in agreement with experimental work on aluminum [12].

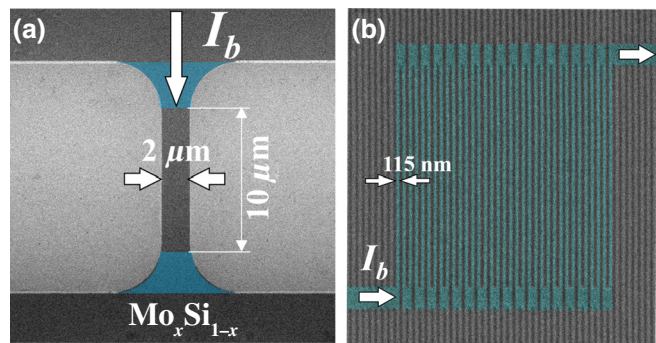


FIG. 1. SEM images of the studied samples. (a) A 2- μm -wide and 10- μm -long straight strip. The black areas denote the α - $\text{Mo}_x\text{Si}_{1-x}$ film and the strip, the gray denotes the etched area, and the blue denotes the areas of $\text{Mo}_x\text{Si}_{1-x}$ designed to prevent the current-crowding effect. (b) A meander comprised of a 115-nm-wide strip line; the total length of the strip line is about 500 μm .

Both samples are patterned by using electron-beam lithography and reactive ion etching. To prevent current-crowding effects at the sharp strip edges, which may lead to an undesirable reduction of the experimentally measured critical current, the two ends of the strip are rounded as depicted in Fig. 1(a). The straight strip is 2 μm wide and 10 μm long, while the meander strip line is 115 nm wide and 500 μm long. The meander strip line is characterized by a filling factor of 0.58. Both samples are characterized by a magnetic field penetration depth $\lambda(0)$ of 708 nm and a Pearl length $\Lambda(0)$ of 303 μm , as calculated from their resistivity and T_c values. These estimates are in line with the values deduced from recent experiments [13,14] and ensure that $w \ll \Lambda(0)$ for both detectors. Here, w is the strip width. Thus, the current distribution is assumed to be homogeneous across both samples.

To verify that the samples detect single photons, a standard statistical analysis of the PCR as a function of the number of incident photons [3] is employed. For Poissonian light sources (cw lasers), in the single-photon regime, the PCR is proportional to the photon flux (or incident light power) in the range from 500 nm to 1550 nm. The setup used for measurements of the PCR and the dark-count rate (DCR) in a magnetic field has been described elsewhere [3]. Light is delivered by a single-mode optical fiber to the sample placed at a distance of 8 cm to create a uniformly illuminated field. An external magnetic field, oriented normally to the plane of the sample, is generated by a superconducting solenoid. All measurements described in what follows are done at $T = 1.7 \text{ K}$. To prevent latching of the wide strip after exceeding the critical current, a shunt resistance of $R = 1 \Omega$ is used. As the shunt is attached to the normal part of the sample, a small part of the current flows through the shunt even when the sample is in the superconducting state, which leads to an

apparent increase of the critical current in photon-counting experiments.

III. RESULTS AND DISCUSSION

A. Critical currents in magnetic field

Figure 2(a) presents the dependence of the critical current I_c of the wide strip on the perpendicular magnetic field B . Specifically, $I_c(B)$ exhibits a linear dependence at low fields and its behavior evolves into a slower nonlinear decrease for fields $B > B^* \simeq 6.9$ mT. This experimental finding resembles that for $I_c(B)$ observed for Nb, NbN, and TaN by Lusche *et al.* [15], Engel *et al.* [16], and Ilin *et al.* [17], as well as for Mo-Ge by Plourde *et al.* [18]. This crossover from the linear law to the nonlinear dependence can be understood as a transition from $I_c(B)$ controlled by the edge barrier for vortex penetration at low fields [18–20] to $I_c(B)$ associated with the bulk pinning of vortices at higher fields [21]. Note that the nearly linear behavior at $B \lesssim 3$ mT means that we are still not fully reaching the depairing current at $B = 0$ as, otherwise, the dependence $I_c(B)$ would, theoretically, be nonlinear, due to the strong pair-breaking effect of the depairing current [22,23]. Indeed, using the parameters of the sample, for zero magnetic field, we calculate a theoretically expected depairing current density of $j_{\text{dep}}(B = 0) = 21 \times 10^9$ A/m². The magnetic field for the suppression of the edge barrier for vortex entry is estimated as $B_s =$

$\Phi_0/2\sqrt{3}\pi\xi w = 11$ mT. Both estimates are neither far from nor very close to the experimental values $j_c(B = 0) = 17 \times 10^9$ A/m² [corresponding to $I_c(B = 0) = 110$ μ A] and $B^* = B_s/2 = 6.5$ mT.

We would like to point out that in our previous work on $\text{Mo}_x\text{Si}_{1-x}$ [9], the critical current density at $T = 1.7$ K in a zero magnetic field was in the range from 15×10^9 A/m² to 18×10^9 A/m², which is about 45%–52% of the depairing critical current density. In that experiment, we used meandering strips with a width of 114 nm. In the present study, we reach critical current densities of about 70% of the depairing current density for the bridge and 64% for the meander strip line.

The dependence $I_c(B)$ for the $\text{Mo}_x\text{Si}_{1-x}$ meander does not follow the edge-barrier model for vortex entry despite quasilinear behavior at low magnetic fields [see Fig. 2(b)] and $I_c(0) \simeq 5.5$ μ A, which is about 64% of the theoretical depairing current. Indeed, from the edge-barrier model [18], it follows that $I_c(0)/I_c(B^*) = 2$, where we estimate $B^* \simeq 95$ mT for the meander (it is 17 times larger than for 2 μ m strip). But from the experiment, we find that I_c drops by a factor of 2 at $B^* \sim 400$ mT. We believe that this difference could be related to the presence of a defect somewhere inside the meander strip line, which may result in a change of the shape of the dependence $I_c(B)$ at low fields even if there is an edge barrier for vortex entry (see, e.g., Fig. 6 in Ref. [24]). Remarkably, for the $\text{Mo}_x\text{Si}_{1-x}$ meander, we do not observe a flux-flow branch in the current-voltage characteristics (the I - V curve) up to $B = 933$ mT [see the inset in Fig. 2(b)], which is much larger than the theoretical estimate $B^* = 95$ mT. By contrast, for the $\text{Mo}_x\text{Si}_{1-x}$ strip, the flux flow branch in the I - V curve appears at approximately $B \gtrsim B^*$ [see the inset in Fig. 2(a)] and its evolution with increasing B is similar to that observed by Samoilov *et al.* [25] for Mo_3Si superconducting strips.

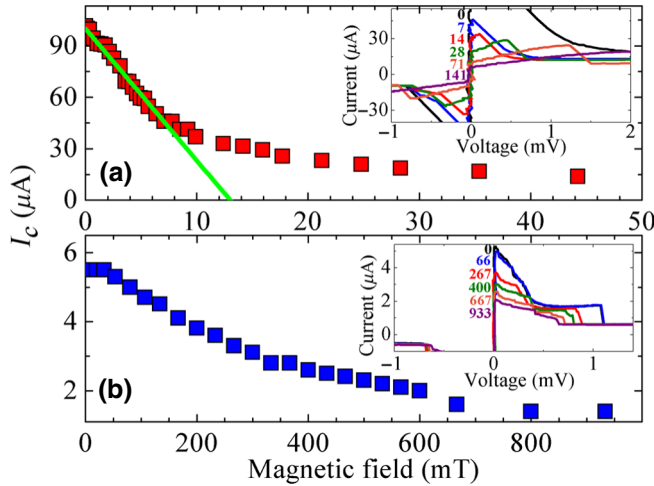


FIG. 2. (a) The dependence of the critical current $I_c(B)$ of the wide $\text{Mo}_x\text{Si}_{1-x}$ strip on the applied magnetic field. The solid line is a fit to the theoretical I_c controlled solely by the edge barrier for vortex entry [18]. (b) The dependence $I_c(B)$ of the $\text{Mo}_x\text{Si}_{1-x}$ meander. The insets show I - V curves for the $\text{Mo}_x\text{Si}_{1-x}$ strip (top) and the meander (bottom) at different magnetic fields in millitesla, as labeled close to the curves. For clarity, only I - V curves recorded with a negative-to-positive voltage sweep are presented. The I - V curves for the wide strip demonstrate a flux-flow regime at $B \gtrsim 10$ mT.

B. Count rates in magnetic field

Figure 3 presents the PCR and the DCR of the wide strip as a function of the bias current and the applied magnetic field for different photon wavelengths. The PCR exhibits a tendency to saturate as $I \rightarrow I_c(B = 0)$ (except for $\lambda = 1550$ nm). The saturation means that we approach 100% intrinsic detection efficiency. In our previous work on micron-wide NbN bridges [3], the saturation of the PCR was only observed on a logarithmic scale and it was tentatively explained by the shape of the constriction-type microbridges that were used. In the present case, the not fully complete saturation on the linear scale is most likely still related to the presence of tapered active areas near the ends of the bridge, which are also exposed to the photon flux. These areas are indicated in blue in the SEM image in Fig. 1(a).

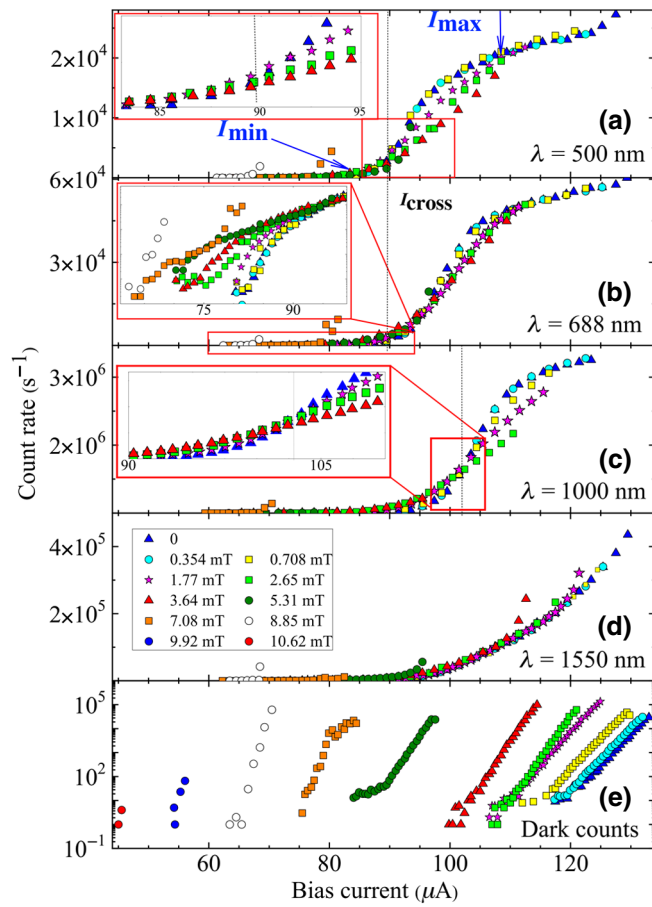


FIG. 3. (a)–(d) The dependence of the PCR of the wide strip on the current at different magnetic fields and for different wavelengths of incident photons. At $B = 0$, the PCR saturates at a relatively large current, except for photons with $\lambda = 1550 \text{ nm}$. One can see the presence of a crossover current I_{cross} for wavelengths 500–1000 nm in (a)–(c), above which the PCR decreases, while for currents $I < I_{\text{cross}}$, the PCR increases with an increasing magnetic field. In (a), the arrows mark the current I_{min} , at which the PCR starts to grow sharply, and I_{max} , at which it is almost saturated. The insets in (a) (linear scale), (b) (logarithmic scale), and (c) (linear scale) show enlarged parts of the regions marked by the red rectangles in semilog scale. (e) The dependence of the DCR on the bias current at different values of B . At $B > 10 \text{ mT}$, dark counts are practically absent.

In the applied magnetic field, the PCR changes gradually as a function of the bias current. Specifically, at small currents the number of counts increases with an increasing magnetic field, whereas at larger currents the PCR decreases with an increasing magnetic field. At intermediate currents, we define a crossover current I_{cross} , as shown in Figs. 3(a)–3(c), at which the PCR is independent of the magnetic field. The crossover current is only observed for wavelengths at which the PCR becomes saturated, as it is indicative of the saturation of the detection efficiency. This peculiar behavior and the presence of the

crossover current are fingerprints of the vortex–antivortex-assisted photon-counting mechanism and the “locality” of the photoresponse in the wide $\text{Mo}_x\text{Si}_{1-x}$ strip.

The evolution of the DCR(I) with an increasing magnetic field is presented in Fig. 3(e). The dependence DCR(I) is similar to that obtained for nanoscale meander-type NbN detectors consisting of 35 connected strips, each having a width of about 100 nm and a length of 7 μm [8]. The origin of the dark counts is assumed to be the occasional entry of vortices due to random processes. According to the London model, at $I \lesssim I_c$ the amplitude of the energy barrier δE varies as $\delta E \sim 1 - I/I_c$ [26]. As the field increases, the linear dependence of $\log(\text{DCR})$ on the current shifts toward lower currents, since I_c decreases with increasing B (see also Fig. 2). Dark counts are practically absent at fields $B > 10 \text{ mT}$, which agrees well with the field at which a low-resistive branch appears in the I - V curve in the inset of Fig. 2(a), identified as a flux-flow regime. At such a low current $I \sim I_c$, the passage of a single vortex across the strip is not enough to heat the sample and, hence, dark counts no longer appear.

To clarify the origin of the crossover current and the dependence of PCR(I) on the magnetic field, in Fig. 4 we present a sketch of the current distribution in a superconducting strip at different values of currents and magnetic fields. Thus, when $B = 0$ the current is distributed uniformly, as depicted by the horizontal lines. In a wide strip, the value of the calculated detection current (defined as a current at which the superconductor switches to a resistive state after absorption of a photon) depends weakly on the coordinate of the incident photon across the strip, except for the areas near the edges with a width of about the diameter of the photon-induced hot spot. This, in particular, contrasts with narrow strips $w \gtrsim D_{\text{HS}}$, in which the detection current varies strongly with the coordinate [27–29]. The uniformity of the current distribution is a consequence of the “locality” of the photoresponse in strips with $w \gg D_{\text{HS}}$. In the theoretical model, it results in an almost steplike dependence of the PCR on the current, which is not observed in the experiment. This difference between experiment and theory may be due to the presence of unavoidable electronic inhomogeneities in the strip or Fano fluctuations, i.e., fluctuations in the number of nonequilibrium quasiparticles produced by the incident photon [30]. Both mechanisms lead to a smeared dependence of the PCR on current. To take this observed “fuzziness” into account, in Fig. 4 we plot a minimal current $I_{\text{min}} = j_{\text{min}}wd$ and a maximal current $I_{\text{max}} = j_{\text{max}}wd$, which are also depicted in Fig. 3. In our simple model, we assume that the probability that the photon will be detected increases smoothly from zero at $I = I_{\text{min}}$, where the current density is equal to j_{min} , up to unity, where the current $I = I_{\text{max}}$ (and the current density is $j = j_{\text{max}}$). So we have a band of bias-current values over which the PCR rises from close to zero to close to 100%.

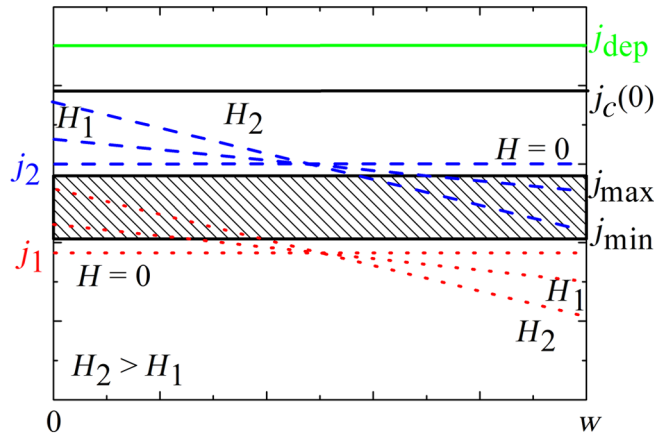


FIG. 4. A graphical representation of the current density across the width of the superconducting strip. The vertical axis represents values of the current density. The upper green line represents the theoretical depairing current density $j_{\text{dep}} = I_{\text{dep}}/wd$, while $j_c(0) = I_c(B=0)/wd$ represents the experimentally deduced critical current density. The range of currents between $I_{\text{min}} = j_{\text{min}}wd$ and $I_{\text{max}} = j_{\text{max}}wd$ represents the band over which the PCR increases nonlinearly from an almost zero value up to the maximal value (see Fig. 3). At the current $I_2 = j_2wd > I_{\text{max}}$ and $H = 0$, the PCR is equal to the maximal value PCR_{max} . At the current $I_1 = j_1wd < I_{\text{min}}$ and $B = 0$, the PCR is equal to zero. An applied magnetic field tilts the current density distribution, leading to a nonuniform response to photons. At $x = 0$ the PCR becomes saturated, whereas at $x = w$ it increases from zero to a finite value. Obviously, the reason is that a perpendicular field adds a current to the bias current at $x = 0$ and subtracts it at $x = w$.

When a perpendicular magnetic field is applied, the supercurrent density distribution becomes nonuniform. Namely, at one edge the current is going out of the plane and at the other edge it is going into the plane. This means that at one edge the current density increases, whereas at the other edge it decreases (see Fig. 4). If the original bias current is larger than I_{max} , in the part of the strip where the current density drops below j_{max} , the PCR will decrease. If the current is less than I_{min} in the part of the strip where the current density is greater than I_{min} , the PCR increases. Between I_{max} and I_{min} , there is a crossover current at which the PCR does not change with the magnetic field. Indeed, such a crossover is observed experimentally for $\lambda = 500$, 688, and 1000 nm. The fact that such a crossover current is not seen for infrared photons with $\lambda = 1550$ nm is most likely related to the absence of saturation in the dependence of $\text{PCR}(I)$.

In contrast to the wide strip, no crossover current is observed for the $\text{Mo}_x\text{Si}_{1-x}$ meander (see Fig. 5) and we also refer to a previous work on narrow $\text{Mo}_x\text{Si}_{1-x}$ meanders [31], where it was also the case that no crossover currents were observed. Note that for the studied wavelengths, single-photon counting starts at approximately the

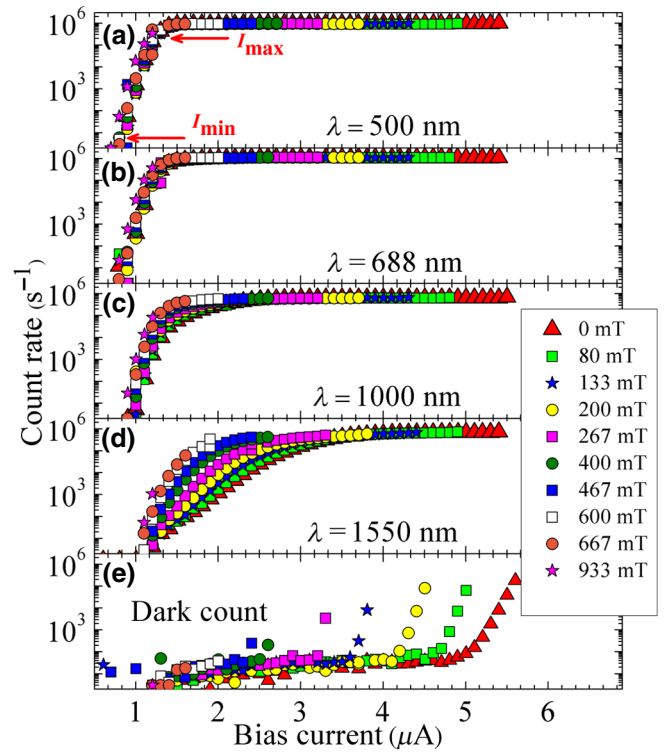


FIG. 5. The PCR vs the bias current in different magnetic fields measured for the $\text{Mo}_x\text{Si}_{1-x}$ meander made of a 115-nm-wide strip line. (a)–(d) Counts for the indicated wavelengths. (e) The dark-count rates. The currents I_{min} and I_{max} , as in Fig. 3, indicate currents at which the PCR starts to grow sharply and saturates, respectively. In contradistinction with Fig. 3, here the data are plotted on a logarithmic scale to emphasize the dependence on the magnetic field, which is hardly visible on a linear scale. The maximum values of the DCR gradually decrease in magnetic fields of 400 mT and above.

same current of approximately $1 \mu\text{A}$, which is close to the retrapping current of the $\text{Mo}_x\text{Si}_{1-x}$ meander $I_r \simeq 0.6 \mu\text{A}$ [see the inset in Fig. 2(b)]. This fact, in conjunction with the found dependence of the PCR on the magnetic field, allows us to suppose that the absorbed photon fully or partially suppresses superconductivity across the whole strip line, forming a hot belt. Indeed, in this case the applied magnetic field should lower the detection current (which does not depend on coordinate) as it does with the critical current [see Fig. 2(b)]. Therefore the dependence $\text{PCR}(I)$ should shift toward lower currents, as follows from Refs. [27,32], and resemble the evolution of $\text{DCR}(I)$ with increasing B . However, since the minimal detection current cannot exceed the retrapping current, as at $I < I_r$, the growing normal domain cannot appear in the superconducting strip [5]. This shift is partially observed only for $\lambda = 1550$ nm. Note that in the wide $\text{Mo}_x\text{Si}_{1-x}$ strip, $I_r = 18 \mu\text{A}$ [see the inset in Fig. 2(a)] and the PCR strongly depends on the magnetic field for all wavelengths.

The crossover current was observed earlier in our previous work on NbN meanders [8] that had almost the same strip-line width as the $\text{Mo}_x\text{Si}_{1-x}$ meander studied here. Because the critical temperature and the thickness of the strip line in the NbN meander are larger than the respective parameters for the $\text{Mo}_x\text{Si}_{1-x}$ one, the diameter of a hot (normal) spot in NbN should be about three times smaller, if one uses the energy-conservation law for its estimation [see Eq. (38) in Ref. [5]]. Therefore, we believe that the “local” model and the vortex-antivortex detection mechanism should determine the photon detection in those NbN meanders too. Because I_{\min} is close to the retrapping current of the NbN strip at $\lambda = 450$ nm, the PCR weakly depends on the magnetic field there [see Fig. 2(d) in Ref. [8]], as in our $\text{Mo}_x\text{Si}_{1-x}$ meander.

Finally, to complete the discussion of the obtained results, we would like to note that the effect of the perpendicular magnetic field on the DCR and the PCR have also been studied by Engel *et al.* [16] and Lusche *et al.* [15] for TaN and NbN meanders with similar strip-line widths. In Ref. [16], no effect of the magnetic field on the PCR was observed at fields up to 10 mT, while the DCR grew as the field value increased. In our $\text{Mo}_x\text{Si}_{1-x}$ meander, the PCR is also changed much more weakly in comparison with the DCR at a fixed current (see Fig. 5), which we attribute to the nonfluctuating nature of the PCR in contrast to the DCR. To find a decrease of the PCR and a crossover current, one needs to be in the regime of PCR saturation, which is indicative of reaching 100% intrinsic detection efficiency, and the width of the superconducting strip should be larger than the diameter of the photon-induced hot spot for applicability of the “local” model. In Ref. [15], the former condition was not fulfilled and only an increase of the PCR was experimentally observed.

IV. CONCLUSIONS

To summarize, we study the PCR in a wide strip and a meander with a narrow strip line made of superconducting $\text{Mo}_x\text{Si}_{1-x}$. We find different dependencies of the PCR on the perpendicular magnetic field in these two systems. Namely, a crossover current I_{cross} is observed for the wide strip, below which the count rate increases with an increasing magnetic field and above which it decreases. This observation is in agreement with the photon-induced vortex-generation model and is explained by the magnetic field induced screening currents in the strip. By contrast, in the narrow $\text{Mo}_x\text{Si}_{1-x}$ meander, no crossover current is observed and the dependence of the PCR on the magnetic field is revealed to be much weaker. We explain this finding as being due to a low value of the detection current, which is close to the retrapping current of the meander, and the photon-induced suppression of superconductivity across the whole width of the meander strip line.

ACKNOWLEDGMENTS

We thank Teunis Klapwijk for stimulating discussions and Gregory Goltsman for his stimulating interest in this work and his encouragement, as well as for the creation of the laboratory infrastructure that we used. This work was supported by the Russian Science Foundation (RSF) Grant No. 17-72-30036 (experimental study of single-photon response of the $\text{Mo}_x\text{Si}_{1-x}$ meander and the strip). The research work of M.Y.M. and O.V.D. was partially conducted within the framework of the COST Action CA16218 (NANOCOBYBRI) of the European Cooperation in Science and Technology (thin-film deposition, structural, and superconducting properties of thin films). D.V. also acknowledges support by the Russian Foundation for Basic Research (RFBR), Grant No. 18-29-20100 (concerning theoretical analysis of experimental results).

-
- [1] G. N. Gol'tsman, O. Okunev, G. Chulkova, A. Lipatov, A. Semenov, K. Smirnov, B. Voronov, A. Dzardanov, C. Williams, and R. Sobolewski, Picosecond superconducting single-photon optical detector, *Appl. Phys. Lett.* **79**, 705 (2001).
 - [2] C. M. Natarajan, M. G. Tanner, and R. H. Hadfield, Superconducting nanowire single-photon detectors: Physics and applications, *Supercond. Sci. Technol.* **25**, 063001 (2012).
 - [3] Y. P. Korneeva, D. Y. Vodolazov, A. V. Semenov, I. N. Florya, N. Simonov, E. Baeva, A. A. Korneev, G. N. Goltsman, and T. M. Klapwijk, Optical Single-Photon Detection in Micrometer-Scale NbN Bridges, *Phys. Rev. Appl.* **9**, 064037 (2018).
 - [4] A. N. Zotova and D. Y. Vodolazov, Photon detection by current-carrying superconducting film: A time-dependent Ginzburg-Landau approach, *Phys. Rev. B* **85**, 024509 (2012).
 - [5] D. Y. Vodolazov, Single-Photon Detection by a Dirty Current-Carrying Superconducting Strip Based on the Kinetic-Equation Approach, *Phys. Rev. Appl.* **7**, 034014 (2017).
 - [6] V. B. Verma, B. Korzh, F. Bussi eres, R. D. Horansky, S. D. Dyer, A. E. Lita, I. Vayshenker, F. Marsili, M. D. Shaw, H. Zbinden, R. P. Mirin, and S. W. Nam, High-efficiency superconducting nanowire single-photon detectors fabricated from mosi thin-films, *Opt. Express* **23**, 33792 (2015).
 - [7] M. Caloz, M. Perrenoud, C. Autebert, B. Korzh, M. Weiss, C. Sch onenberger, R. J. Warburton, H. Zbinden, and F. Bussi eres, High-detection efficiency and low-timing jitter with amorphous superconducting nanowire single-photon detectors, *Appl. Phys. Lett.* **112**, 061103 (2018).
 - [8] D. Y. Vodolazov, Y. P. Korneeva, A. V. Semenov, A. A. Korneev, and G. N. Goltsman, Vortex-assisted mechanism of photon counting in a superconducting nanowire single-photon detector revealed by external magnetic field, *Phys. Rev. B* **92**, 104503 (2015).
 - [9] Y. P. Korneeva, M. Y. Mikhailov, Y. P. Pershin, N. N. Manova, A. V. Divochiy, Y. B. Vakhtomin, A. A. Korneev, K. V. Smirnov, A. G. Sivakov, A. Y. Devizenko, and G. N.

- Goltsman, Superconducting single-photon detector made of MoSi film, *Supercond. Sci. Technol.* **27**, 095012 (2014).
- [10] H. Bartolf, *Fluctuation Mechanisms in Superconductors* (Springer Spektrum, Springer Fachmedien Wiesbaden, Germany, 2016).
- [11] J. R. Clem and V. G. Kogan, Kinetic impedance and depairing in thin and narrow superconducting films, *Phys. Rev. B* **86**, 174521 (2012).
- [12] J. Romijn, T. M. Klapwijk, M. J. Renne, and J. E. Mooij, Critical pair-breaking current in superconducting aluminum strips far below t_c , *Phys. Rev. B* **26**, 3648 (1982).
- [13] X. Zhang, A. E. Lita, K. Smirnov, H. Liu, D. Zhu, V. B. Verma, S. W. Nam, and A. Schilling, Strong suppression of the resistivity near the transition to superconductivity in narrow micro-bridges in external magnetic fields, e-print, eid arXiv:1909.02915 (2019), arXiv:1909.02915 [cond-mat.supr-con].
- [14] L. Ceccarelli, D. Vasyukov, M. Wyss, G. Romagnoli, N. Rossi, L. Moser, and M. Poggio, Imaging pinning and expulsion of individual superconducting vortices in amorphous MoSi thin films, *Phys. Rev. B* **100**, 104504 (2019).
- [15] R. Lusche, A. Semenov, Y. Korneeva, A. Trifonov, A. Korneev, G. Gol'tsman, and H.-W. Hübers, Effect of magnetic field on the photon detection in thin superconducting meander structures, *Phys. Rev. B* **89**, 104513 (2014).
- [16] A. Engel, A. Schilling, K. Il'in, and M. Siegel, Dependence of count rate on magnetic field in superconducting thin-film TaN single-photon detectors, *Phys. Rev. B* **86**, 140506 (2012).
- [17] K. Ilin, D. Henrich, Y. Luck, Y. Liang, M. Siegel, and D. Y. Vodolazov, Critical current of Nb, NbN, and TaN thin-film bridges with and without geometrical nonuniformities in a magnetic field, *Phys. Rev. B* **89**, 184511 (2014).
- [18] B. L. T. Plourde, D. J. Van Harlingen, D. Y. Vodolazov, R. Besseling, M. B. S. Hesselberth, and P. H. Kes, Influence of edge barriers on vortex dynamics in thin weak-pinning superconducting strips, *Phys. Rev. B* **64**, 014503 (2001).
- [19] M. Y. Kupriyanov and K. K. Likharev, Effect of an edge barrier on the critical current of a superconducting film, *Sov. Phys. Solid State* **16**, 1835 (1975).
- [20] M. Benkraouda and J. R. Clem, Critical current from surface barriers in type-II superconducting strips, *Phys. Rev. B* **58**, 15103 (1998).
- [21] A. A. Elistratov, D. Y. Vodolazov, I. L. Maksimov, and J. R. Clem, Field-dependent critical current in type-II superconducting strips: Combined effect of bulk pinning and geometrical edge barrier, *Phys. Rev. B* **66**, 220506 (2002).
- [22] G. M. Maksimova, N. V. Zhelezina, and I. L. Maksimov, Critical current and negative magnetoresistance of superconducting film with edge barrier, *Europhys. Lett.* **53**, 639 (2001).
- [23] V. P. Andratskii, L. M. Grundel', V. N. Gubankov, and N. B. Pavlov, Destruction of superconductivity in thin narrow films by a current, *Sov. Phys. JETP* **38**, 794 (1974).
- [24] D. Y. Vodolazov, K. Ilin, M. Merker, and M. Siegel, Defect-controlled vortex generation in current-carrying narrow superconducting strips, *Supercond. Sci. Technol.* **29**, 025002 (2015).
- [25] A. V. Samoilov, M. Konczykowski, N. C. Yeh, S. Berry, and C. C. Tsuei, Electric-Field-Induced Electronic Instability in Amorphous Mo₃Si Superconducting Films, *Phys. Rev. Lett.* **75**, 4118 (1995).
- [26] H. Bartolf, A. Engel, A. Schilling, K. Il'in, M. Siegel, H.-W. Hübers, and A. Semenov, Current-assisted thermally activated flux liberation in ultrathin nanopatterned NbN superconducting meander structures, *Phys. Rev. B* **81**, 024502 (2010).
- [27] A. N. Zotova and D. Y. Vodolazov, Intrinsic detection efficiency of superconducting nanowire single photon detector in the modified hot spot model, *Supercond. Sci. Technol.* **27**, 125001 (2014).
- [28] A. Engel, J. Lonsky, X. Zhang, and A. Schilling, Detection mechanism in SNSPD: Numerical results of a conceptually simple, yet powerful detection model, *IEEE Trans. Appl. Supercond.* **25**, 2200407 (2015).
- [29] J. J. Renema, Q. Wang, R. Gaudio, I. Komen, K. Op't Hoog, D. Sahin, A. Schilling, M. P. van Exter, A. Fiore, A. Engel, and M. J. A. de Dood, Position-dependent local detection efficiency in a nanowire superconducting single-photon detector, *Nano Lett.* **15**, 4541 (2015).
- [30] A. G. Kozorezov, C. Lambert, F. Marsili, M. J. Stevens, V. B. Verma, J. P. Allmaras, M. D. Shaw, R. P. Mirin, and S. W. Nam, Fano fluctuations in superconducting-nanowire single-photon detectors, *Phys. Rev. B* **96**, 054507 (2017).
- [31] A. A. Korneev, Y. P. Korneeva, M. Y. Mikhailov, Y. P. Pershin, A. V. Semenov, D. Y. Vodolazov, A. V. Divochiiy, Y. B. Vakhtomin, K. V. Smirnov, A. G. Sivakov, A. Y. Devizenko, and G. N. Goltsman, Characterization of MoSi superconducting single-photon detectors in the magnetic field, *IEEE Trans. Appl. Supercond.* **25**, 2200504 (2015).
- [32] L. N. Bulaevskii, M. J. Graf, and V. G. Kogan, Vortex-assisted photon counts and their magnetic field dependence in single-photon superconducting detectors, *Phys. Rev. B* **85**, 014505 (2012).